Title

On the valence fluctuation in the early actinide metals

Authors

Söderlind, P

Landa, A

Tobin, JG

et al.

Publication Date

2016-02-01

DOI

10.1016/j.elspec.2015.11.014

LAWRENCE
LIVERMORE
NATIONAL
LABORATORY

LLNL-JRNL-672996

ON THE VALENCE FLUCTUATION IN THE EARLY ACTINIDE METALS

P. Soderlind, A. Landa, J. G. Tobin, P. Allen, S. Medling, C. H. Booth, E. D. Bauer, J. C. Cooley, D. Sokaras, T. -C. Weng, D. Nordlund

June 11, 2015

Journal of Electron Spectroscopy and Related Phenomena

On the valence fluctuation in the early actinide metals

P. Söderlind, A. Landa, J. G. Tobin, and P. Allen,
Lawrence Livermore National Laboratory, Livermore, CA 94550, USA

S. Medling, C. H. Booth,
Lawrence Berkeley National Laboratory, Berkeley, CA 94720, USA

E. D. Bauer, J. C. Cooley
Los Alamos National Laboratory, Los Alamos, NM 87545, USA

D. Sokaras, T.–C. Weng, and D. Nordlund,
Stanford Synchrotron Radiation Lightsource, SLAC National Laboratory,
Menlo Park, CA 94025, USA

Abstract

Recent x-ray measurements suggest a degree of valence fluctuation in plutonium and uranium intermetallics. We are applying a novel scheme, in conjunction with density functional theory, to predict 5f configuration fractions of states with valence fluctuations for the early actinide metals. For this purpose we perform constrained integer f-occupation calculations for the α phases of uranium, neptunium, and plutonium metals. For plutonium we also investigate the δ phase. The model predicts uranium and neptunium to be dominated by the f^3 and f^4 configurations, respectively, with only minor contributions from other configurations. For plutonium (both α and δ phase) the scenario is dramatically different. Here, the calculations predict a relatively even distribution between three valence configurations. The δ phase has a greater configuration fraction of f^6 compared to that of the α phase. The theory is consistent with the interpretations of modern x-ray experiments and we present resonant x-ray emission spectroscopy results for α-uranium.

The electronic structures of the actinide metals and actinide-based compounds and alloys remain subjects for intense discussions and research. As regards the metals, the conventional view has been that the early actinides, thorium-plutonium, possess relatively weakly correlated f electrons so that a valence-band picture of these states is appropriate. This view is certainly correct for α-Pu while the situation in δ-Pu has been debated for many years. Of course, the late actinide metals (americium and beyond) have 5f states that are best described as localized and atomic like. Many experimental and theoretical approaches have been applied to better understand the nature of the electronic structure and the 5f electrons in particular. For a review see Moore and van der Laan [1].

The concept of fluctuating valence configurations has recently been expanded by x-ray emission and absorption studies [2, 3] that have been able to assign weights (or fractions) to these configurations for actinides and their intermetallics. Because of the numerous successes of density-functional-theory (DFT) calculations for the actinide metals [4] we have leveraged this framework in conjunction with a novel scheme that includes constrained electronic configurations to illuminate the possibilities of valence fluctuations in the early actinide metals (uranium through plutonium).

The idea is to perform constrained calculations that represent integer occupation f configurations and then determine their respective fractions such that the resulting multiconfigurational state, averaged over the fluctuations, reproduces the unconstrained DFT result. The scheme is currently limited to study up to three integer configurations with unknown fractions, *a*, *b*, and *c*. These three unknowns can be determined from solving this set of linear equations for the configurations f^{α}, f^{β}, and f^{γ}:

$$a + b + c = 1 \tag{1}$$

$$a\alpha + b\beta + c\gamma = \xi \tag{2}$$

$$ap^{\alpha} + bp^{\beta} + cp^{\gamma} = 0 \tag{3}$$

Here, ξ is the unconstrained (non-integer) DFT f occupation, p^{α}, p^{β}, and p^{γ} are the electronic pressures associated with configurations f^{α}, f^{β}, and f^{γ}. These pressures are calculated at the equilibrium volume of the unconstrained calculations and Eq. (3) thus ensures that the valence

fluctuations do not produce a net hydrostatic pressure. Of course, another condition is that these fractions cannot be negative, i.e., a, b, and $c \geq 0$.

In principal, one may choose another quantity than the electronic pressure (p) in Eq. (3), such as atomic volume, atomic density, or total energy, to help determine the fractions a, b, and c. Our choice is made because the pressures better represent the instantaneous homogenous distribution of all configurations on each atom than the atomic volumes or densities do. The volume (and density) is rather a reflection of the electronic pressure and a relaxation process. The reason the energy is not applied in lieu of the pressure is purely technical, as the constrained treatments do now allow for a comparison of their total energies as discussed below.

The integer, f^i (i = 2, 3, 4, 5, 6), configurations are modeled simply by constraining the overall number of valence electrons. A conventional treatment for plutonium, for example, include 16 valence electrons (6s, 6p, 7s, 7p, 6d, and 5f states) and with a 5f-band occupation of about 5.3 (see Table I). Reducing the number of valence electrons to 15.2 reproduces the integer f^5 configuration while increasing it to 16.4 results in an f^6 configuration. To maintain charge neutrality in the system (ionization does not take place) the number of protons in the nucleus is adjusted with the constrained number of valence electrons. This procedure ensures that the total energy is consistently calculated for a charge neutral system and thus allowing for determination of accurate electronic pressures. The absolute total energy itself, however, cannot be compared between the various configurations because of the difference in nuclear and valence charge.

The most accurate DFT calculations for the actinide metals involve so-called full potential all-electron treatments of the electronic structure and energy, see for example [5]. For entirely technical reasons, full-potential methods usually accomplish the exact geometrical description of the electronic structure, “full potential”, by dividing the crystal into non-touching spheres centered at each atom site with an interstitial region in between. Because of this construct, the interstitial charge is not associated with an atomic orbital such as the 5f orbital and therefore this technicality underestimates the true 5f-band occupation a small amount as discussed in detail earlier [6]. To correct for this we employ calculations that do not utilize interstitial charges similar to those we have done previously for americium where the occupation numbers were the main focus [6]. From these non-full-potential electronic structures the integer 5f-occupation constraints were determined.

For the best possible electronic structure and total energy we utilize an accurate, fully relativistic, full-potential methodology [5, 7] that includes the orbital-polarization correction as was done previously for plutonium [7, 8]. The calculations for these actinide metals are identical, except for the crystal structures that are orthorhombic, Cmcm, primitive orthorhombic, Pnma, monoclinic, $p2_1/m$, and face-centered cubic, cF4, for α-U, α-Np, α-Pu, and δ-Pu, respectively [9]. The plutonium phases develop magnetic spin and orbital moments that are anti-ferromagnetic (α) and paramagnetic (δ), described in detail by Söderlind and Sadigh [7].

The procedure to calculate the configurational fractions is illustrated for α-U in Fig. 1. The total energies of α-U subject to the constrained f^2, f^3, and f^4 configurations (also in the α-U crystal structure) are plotted versus atomic volume. The α-U equilibrium volume is 20.67 $Å^3$ (see Table II) and is marked by a dashed vertical line. Because the equilibrium volumes of the f^3 and f^4 configurations are very close to that of α-U, their respective electronic pressure at 20.67 $Å^3$ is quite small (-1.6 and -0.2 GPa). The f^2 configuration, on the other hand, has a substantially larger equilibrium volume that implies a relatively large electronic pressure (19.5 GPa) at the α-U equilibrium volume. The f^4 state cannot compensate for the f^2 configuration in terms the electronic pressures and consequently the configurational fraction of f^4 vanishes, see Table I.

For both α-Pu and δ-Pu all (f^4, f^5, and f^6) valence configurations have fairly similar bonding characteristics leading to electronic pressure components (p^4, p^5, and p^6) that are small and close in magnitude. This is a prerequisite for valence fluctuations in our model. Clearly, the model depends on accurate calculations of these electronic pressure components. Fortunately, for the early actinide metals, the theoretical equilibrium volumes and bulk moduli are in very good agreement with experiments: See Table II. Both the α and the δ phases of plutonium are dominated by the f^5 and f^6 valence states in the model with relatively small amount of f^4. The f^5 state is also more prevalent in the α phase and this is in good quantitative agreement with the interpretations of earlier x-ray emission spectroscopy [2, 3].

We also conduct new resonant x-ray emission spectroscopy (RXES) measurements on α-U samples for comparison with the theoretical model. These samples are purified from starting material that already had decay products removed by an isotopic separation process that yields depleted, low-carbon uranium metal with significant Mg and Ca fluorite inclusions. Removal of these volatile fluorites to levels below 10-20 ppm is accomplished by melting ~ 1 inch thick

chunks of the starting material in a graphite crucible in a vacuum induction furnace for about 1 hour. The vacuum level during casting is between 300 and 400 mTorr with a leak rate of less than 5 mTorr per minute. The graphite crucible, stopper rod, and mold are all yttria coated to prevent reaction of the uranium with the graphite. The graphite crucible, charge, and mold are heated in an induction coil driven at ~ 2kHz, with power levels up to 80kW. Heating continues until the uranium charge melts and has reached a temperature of 1400 °C. The temperature is then reduced to ~ 1300 °C. The melt is held at ~1300 °C for an hour, after which the stopper rod is lifted allowing the molten metal to flow through the centerline hole of the crucible and down into the 800 °C mold. The crucible is at the center of the length of the induction coil where heating is maximized. The mold is, by design, half in and half out of the coil and therefore heats more slowly and is hotter at the top. For this casting the pour time is about 30 seconds and the heat is left on during the pour. The casting is allowed to cool to room temperature overnight, after which the casting is removed from the mold. Cut bars were etched in a hot fifty-fifty solution of HNO_3 and H_2O to remove brass deposited on the surface by the cutting process. The primary α-U sample was etched in concentrated HNO_3 prior to loading into the sample holder for the x-ray emission experiments (see below).

The measurements were collected on BL 6-2 at the Stanford Synchrotron Radiation Lightsource at the U L_{III} edge using a half-tuned Si(311) double-crystal monochromator and a 7-crystal Johann-type spectrometer [10]. Emission data are collected as a function of incident and emitted energy at the U $L_{\alpha 1}$ line (~13.6 keV). The spectrometer is energy calibrated by setting the monochromator to the first inflection point of the Au L_{II} edge from the absorption of a gold reference foil, and then defining the energy of the direct scattered beam into the spectrometer to be 13734 eV. The incident energy is then calibrated such that the first infection point of the *K*-edge absorption from a zirconium reference foil is 17998 eV. The spectrometer resolution is measured to be 1.4 eV, including the monochromator resolution. Samples of α-U and UO_2 are loaded into a liquid helium flow cryostat, and data are collected at 20 K and room temperature. These data are compared to previous data collected on UCd_{11} [2], and UF_4 [11] below, that are recalibrated in energy for direct comparison to our new data. All data are corrected for self-absorption of the emitted photon in the matrix [3].

RXES data are fitted to the Kramers-Heisenberg equation of the form:

$$I_e(E_i, E_t) = \int d\varepsilon\, \eta(\varepsilon) \frac{A}{(E_{gi} - \varepsilon + E_i)^2 + \Gamma_i^2/4} \cdot \times \frac{\Gamma_f/(2\pi)}{(E_{if} - \varepsilon + E_t)^2 + \Gamma_f^2/4}$$

This form is simplified to account for the measurements presented here, namely, with an intermediate state that includes an excited state 6d electron and a hole in the $2p_{3/2}$ shell, and a final state with the excited 6d electron where the $2p_{3/2}$ shell is filled by a decay from the $5d_{5/2}$ shell (the U $L_{\alpha 1}$ fluorescence). In addition, the transition matrix element A from the ground-to-intermediate state excitation and the intermediate-to-final state decay is assumed to be constant, which is a reasonable assumption since the intermediate state is dominated by empty 6d states above the Fermi energy. Here I_e is the emitted intensity, E_i is the incident photon energy, E_t is the transfer energy E_t=E_i-E_e, E_e is the emitted photon energy, $\eta(\varepsilon)$ is the local unoccupied partial density of states (upDOS), E_{gi} is an offset energy representing the energy difference between the ground and an intermediate state, E_{if} is an offset energy representing the energy difference between an intermediate and the final state, Γ_i is a broadening term due primarily to the core-hole lifetime of the initial excitation (the $2p_{3/2}$ core hole here), and Γ_f is a broadening term due primarily to the core-hole lifetime of the final excitation (the $3d_{3/2}$ core hole here).

The upDOS is parameterized as described previously, by assuming a peak in the d states near the Fermi level followed by a fairly featureless continuum as characterized by an energy position and a width σ. In the case of an intermediate valent system (i.e. multiconfigurations), the f-orbital components can be split in the presence of a core hole. These components screen the core hole differently, thereby potentially splitting the aforementioned d states near the Fermi level. Note that splitting only occurs if the Coulomb interaction U between the core hole and the different f configurations is larger than the binding energy of whatever is causing them to be degenerate, eg. the Kondo effect [12]. If U is too low, for instance, if f-orbital delocalization reduces U sufficiently, one would expect a single peak shifted from, say, the expected localized f^3 position. As will be demonstrated below, at the very least we observe a shifted but strongly broadened peak, and we therefore model this spectra assuming the upDOS is composed of three components, corresponding to f^2, f^3, and f^4 contributions [3].

Even though the high x-ray energies used here generally suggest a bulk measurement, since α-U is easily oxidized, data reported below are from the most recent synthesis, including a nitric acid wash to remove any oxide layer approximately two days before RXES measurements.

An older sample that had been allowed to oxidize over several years was also measured both before and after an acid wash. All α-U RXES data are indistinguishable within error estimates while easily distinguishable from data on UO_2, and so we conclude that little, if any, contamination by an oxide layer has affected the RXES data.

Figure 2 shows the RXES data at various incident energies. The α-U data should be compared primarily to the UCd_{11} and UF_4 data as examples of nearly pure, localized f^3 and f^2 compounds, respectively. The UO_2 data is significantly broadened by crystal field states [11], and is shown as an example of large crystal field splitting. The α-U data encompasses the range defined by the UCd_{11} and UF_4 data, indicating a strong f^3 component and a likely mixture of f^2 states. It is important to note that in this style of plotting, where the data below the threshold energy E_0 of about 17170 eV as indicated by its lack of dispersion in E_t with E_i is normalized to the peak emission, that the higher normalized emission of α-U above ~3565 eV is an artifact of the normalization procedure and does not actually indicate an increase in emission flux.

Given these profiles, it is also important to note that any delocalization of an orbital manifests itself in these spectra as a shift to higher energy and possible peak broadening, as the reduced screening of the core hole increases the Coulomb interaction between the outgoing photoelectron and the core hole, thereby increasing the energy required for the photoelectron to escape the influence of the absorbing atom. The significant negative shift in the peak emission energy of α-U compared to UF_4 therefore indicates a very significant, possibly dominant f^3 contribution.

Fits of the upDOS to these data quantify some of these conclusions. The fit results for the α-U spectra are shown in Figure 3 and the resulting upDOS is shown Figure 4. The fit parameters are summarized in Table III. Of particular interest is the value of E_{gi} for α-U relative to the other reference materials. E_{gi} for the reference materials is relatively fixed in energy near 3560 eV. UO_2 appears slightly lower, but this shift is attributable to the crystal field split states, which are not included in the fit. E_{gi} for α-U, on the other hand, is about 2 eV higher. As mentioned above, this positive shift is a probable indication of a more delocalized f-orbital. Moreover, the width of the peaks used to model the upDOS, given as σ in Table III, shows sharp transitions for UF_4 (1.4 eV) and UCd_{11} (2.0 eV), somewhat broadened for UO_2 (2.7 eV) as expected from crystal field splitting of the d-orbital, and even broader transitions for α-U (3.4

eV). Since crystal field splitting of the d-orbital in α-U is unlikely to be as large as for UO_2, we must conclude that the broad line shape is due to f-orbital delocalization. Of course, important for the context of this paper, the fits provide an estimate of the f-configuration occupancies, which allow an estimate of the average f-occupancy, $n_f = 2.54 \pm 0.04$.

All reported errors are based on assuming contributions to the resulting fit's χ^2 is randomly distributed. There are sources of systematic error that could have an effect on these conclusions. The most important potential source is that we assume an upDOS in the ground state that is peaked near the Fermi level, but is otherwise fairly featureless. This is clearly not the case in UO_2, although the features in the UO_2 spectra mainly contribute to the peak broadening parameter σ and have little effect on the estimate of n_f. Another potential source is the nature of the delocalization of the f-orbital that is reflected in the α-U fit results as the shift in E_{gi} and the large σ. If delocalization introduces further structure into the emission line shape, it is most likely that our estimate of $n_f = 2.54$ is a lower-bound estimate, comparing well with our calculations suggesting $n_f \sim 2.9$, see Table I. In the theoretical model the f orbitals are indeed well delocalized and a somewhat larger n_f is therefore understandable.

In summary, we have calculated the configurational fractions in the valence-fluctuation state of the early actinides. In this novel approach, the fluctuations are due to hopping of electrons between atoms that are described in the model by DFT band states. The conclusion is that uranium and neptunium show weak fluctuations and plutonium (both α and δ) shows strong fluctuations. The presented technique is applicable for the early actinides because the 5f electrons are appropriately modeled by density-functional theory [18]. For systems with more localized and atomic-like f-electron states, such as the rare-earth metals or the late actinides (americium and on), the present approach may be less relevant and methods designed for strongly correlated electrons more suitable [18, 19]. We have furthermore utilized RXES for α-U and after a careful analysis arrived at a lower bound for the average f occupation close to 2.54 in reasonably consistent with the presented theoretical model. Uranium L_{III}-edge, $L_{\alpha 1}$ RXES measurements indicate a mixed f^2 and f^3 configuration for α-U with strong delocalization of the f-orbital also in good agreement with the theoretical analysis.

Acknowledgments

We thank B. Sadigh for helpful discussion. This work was performed under the auspices of the U.S. DOE by LLNL under Contract DE-AC52-07NA27344. Work at Lawrence Berkeley National Laboratory supported by the Director, Office of Science, Office of Basic Energy Sciences (OBES), of the U.S. Department of Energy (DOE) under Contract No. DE-AC02-05CH11231. Sample preparation at Los Alamos National Laboratory (LANL) was performed under the auspices of the U.S. DOE, OBES, Division of Materials Sciences and Engineering. X-ray absorption and RXES data were collected at the Stanford Synchrotron Radiation Lightsource, a national user facility operated by Stanford University on behalf of the DOE, Office of Basic Energy Sciences.

References

[1] K. T. Moore, G. van der Laan, Rev. Mod. Phys. 81, 235 (2009).

[2] C. H. Booth et al., Proc. Natl. Acad. Sci. U. S. A. 109, 1-205 (2012).

[3] C. H. Booth et al., J. Electron. Spectr. Rel. Phenom. 194, 57 (2014).

[4] P. Söderlind, J. Electron. Spectr. Rel. Phenom. 194, 2 (2014).

[5] J. M. Wills, O. Eriksson, M. Alouani, and D. L. Price in *Electronic Structure and Physical Properties of Solids*, ed. H. Dreysse (Springer-Verlag, Berlin, 1998), p. 148.

[6] P. Söderlind, K. T. Moore, A. Landa, B. Sadigh, and J. A. Bradley, Phys. Rev. B 84, 075138 (2011).

[7] P. Söderlind and B. Sadigh, Phys. Rev. Lett. 92, 185702 (2004).

[8] P. Söderlind, Phys. Rev. B 77, 085101 (2008).

[9] J. Donohue, *The Structure of the Elements*, (Wiley, New York, 1974).

[10] D. Sokaras, T. C. Weng, D. Nordlund, R. Alonso-Mori, P. Velikov, D. Wenger, A. Garachtchenko, M. George, V. Borzenets, B. Johnson, T. Rabedeau and U. Bergmann, Review of Scientific Instruments 84 (2013).

[11] J. G. Tobin, S. W. Yu, C. H. Booth, T. Tyliszczak, D. K. Shuh, G. van der Laan, D. Sokaras, D. Nordlund, T. C. Weng and P. S. Bagus, Phys. Rev. B 92 (2015).

[12] W. Kohn and T. K. Lee, Phil. Mag. A 45, 313 (1982).

[13] S. Dabos, C. Dufour, U. Benedict, and M. Pagès, J. Magn. Magn. Mater. 63 & 64, 661 (1987).

[14] S. Dabos-Seignon, J. P. Dancausse, E. Gering, S. Heathman, and U. Benedict, J. Alloys Compd. 190, 237 (1993).

[15] Ph. Faure and C. Genestier, J. Nucl. Mater. 385, 38 (2009).

[16] Ph. Faure and C. Genestier, J. Nucl. Mater. 397, 74 (2010).

[17] Y. Zhao, J. Zhang, D. W. Brown, D. R. Korzekwa, R. S. Hixon, L. Wang, Phys. Rev. B 75, 174104 (2007).

[18] P. Söderlind, G. Kotliar, K. Haule, P. M. Oppeneer, and D. Guillaumont, MRS Bull. 35, 883 (2010).

[19] S. Y. Savrasov, K. Haule, G. Kotliar, Phys. Rev. Lett. 96, 024109 (2006).

Tables

Table I. Calculated *f*-orbital occupancies (n_f) and configurational fractions (f^n) at ambient pressure.

Material	n_f	f^2	f^3	f^4	f^5	f^6
α-U	2.91	0.09	0.91	0	0	0
α-Np	4.16	0	0	0.84	0.16	0
α-Pu	5.31	0	0	0.11	0.49	0.40
δ-Pu	5.31	0	0	0.17	0.34	0.49

Table II. Atomic volume (Å^3) and bulk modulus (GPa). Experimental data are obtained at room temperature and shown in the parenthesis. The experimental bulk modulus for δ-Pu is from a measurement of a δ-Pu-2.3at.%Ga alloy. All experimental data are taken from Refs. [9,13-17].

Material	Atomic volume	Bulk modulus
α-U	20.67 (20.75)	133 (119)
α-Np	19.16 (19.21)	157 (120)
α-Pu	20.30 (20.08)	45.0 (43)
δ-Pu	24.90 (24.82)	41.0 (30)

Table III. RXES fit results. E_{gi} and E_{gf} are defined in these fits to correspond to the f^2 resonance. The energy separation between the f^2 and f^3 resonances and the f^3 and the f^4 resonances, was defined to be 7.2 eV as determined from the fits to the UCd_{11} data and the UF_4 data. The energy of the f^2 component is arbitrarily fixed to E_{gi} for these fits.

sample	$\mathbf{E_{gi}}$	$\mathbf{E_{gf}}$	$\mathbf{\Gamma_i}$	$\mathbf{\Gamma_f}$	$\mathbf{f_2}$	$\mathbf{f_3}$	$\mathbf{f_4}$	$\boldsymbol{\sigma}$	**r/s**	$\mathbf{n_f}$
UCd_{11}	17175.0(2)	3559.9(2)	8.4(4)	3.0(1)	1.2(2)	6.3(4)	0.0(1)	2.0(2)	3.2(2)	2.83(3)
UF_4	17174.3(1)	3560.4(1)	7.6(1)	3.4(1)	1.8(2)	0.1(1)	0.0(1)	1.4(5)	9.1(5)	2.1(1)
UO_2	17174.8(1)	3558.7(1)	7.5(1)	3.1(1)	3.1(3)	0.2(1)	0.0(1)	2.7(4)	3.7(3)	2.06(7)
α-U	17177.5(1)	3562.3(1)	8.9(1)	1.7(1)	6.1(2)	7.2(9)	0.0(1)	3.4(2)	1.2(4)	2.54(4)

Figure Captions

1. Calculated total energies (shifted to zero for the energy minima) as functions of atomic volume for the constrained f^2 (blue), f^3 (purple), and f^4 (red) configurations and α-U. The vertical dashed line shows the equilibrium volume for α-U (20.67 $Å^3$). The electronic pressures (p^2, p^3, and p^4 in GPa) are indicated in the figure.

2. RXES data as a function of E_i and E_t for UF_4 (black), UCd_{11} (red), UO_2 (dotted black), and α-U (blue). The α-U data are collected at 20 K, while the data from other materials are used as reference and collected at room temperature. No temperature dependence is observed. The emission flux is plotted at fixed E_i (as indicated by the offset), but is normalized to the maximum emission at that E_i. With this normalization, the very low emitted intensities below the uranium L_{III} threshold energy E_0 are thus plotted on the same scale as the high emitted intensities above E_0.

3. Fit result for α-U RXES data, displayed with the same normalization as Fig. 2.

4. Unoccupied partial density of states (upDOS) determined to fits to RXES data on α-U. The upDOS is parameterized into three main components that are attributed to the f^2, f^3, and f^4 configurations; however, the f^4 component is not included in this figure since the contribution is so small.

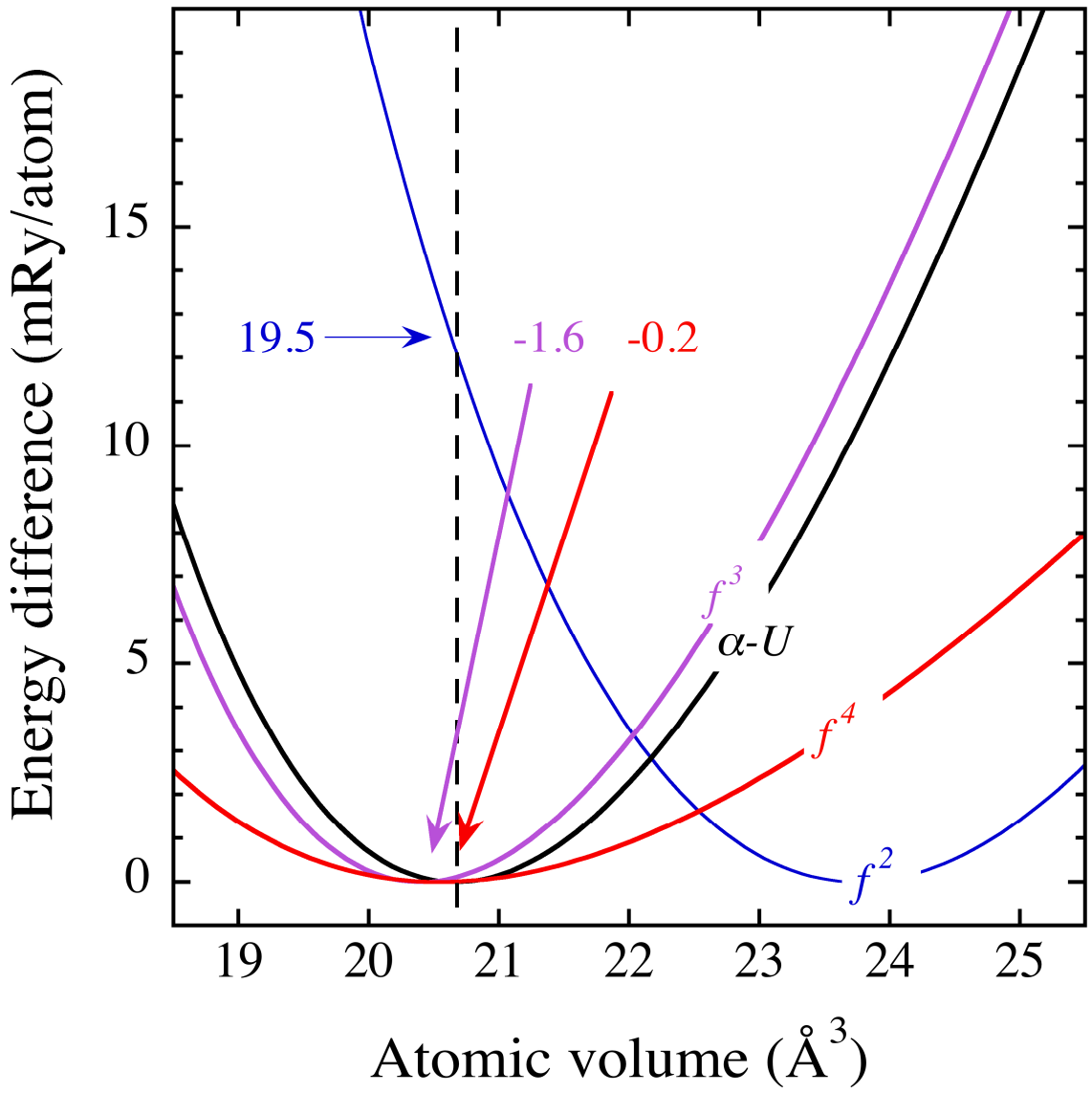
Energy difference (mRy/atom)
15
10
5
0
19
20
21
22
23
24
25
Atomic volume (Å^3)
19.5
-1.6
-0.2
f^3
α-U
f^4
f^2

Fig. 1

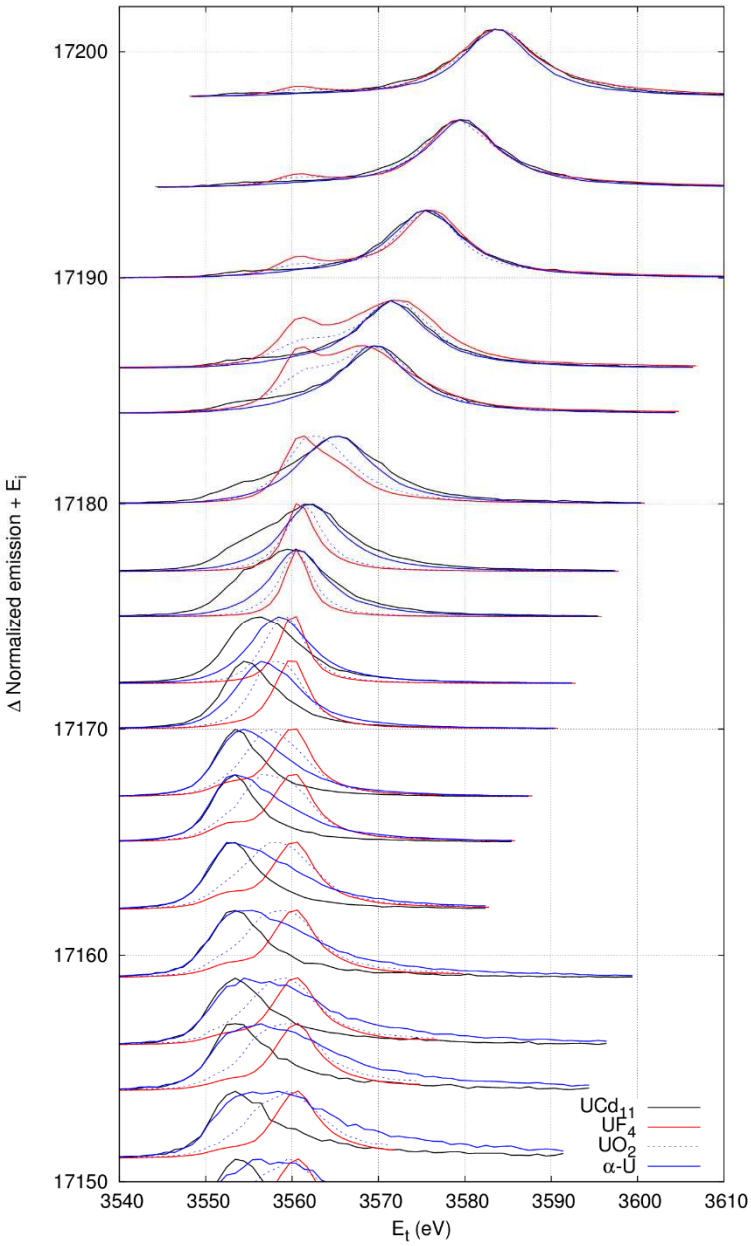
17200
17190
17180
17170
17160
17150
Δ Normalized emission + E_i
3540
3550
3560
3570
3580
3590
3600
3610
E_t (eV)
UCd11
UF4
UO2
α-U

Fig. 2

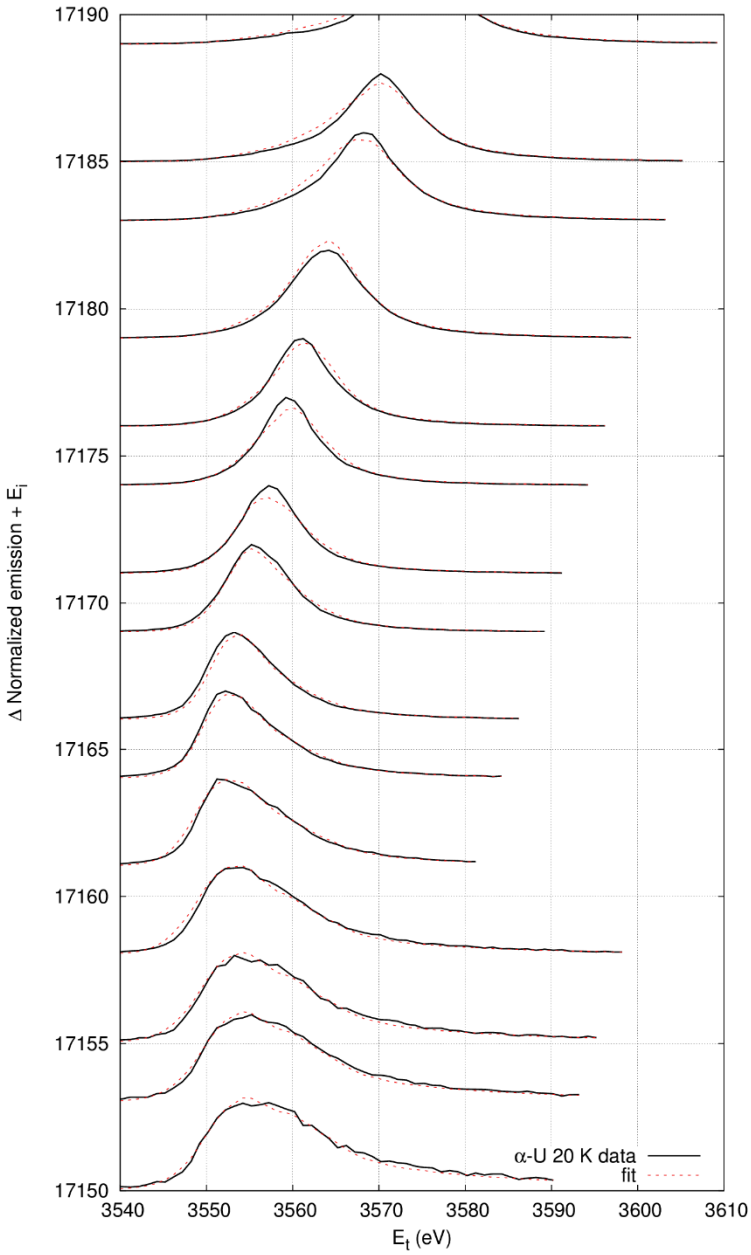
17190
17185
17180
17175
17170
17165
17160
17155
17150
Δ Normalized emission + E_i
3540
3550
3560
3570
3580
3590
3600
3610
E_t (eV)
α-U 20 K data
fit

Fig. 3

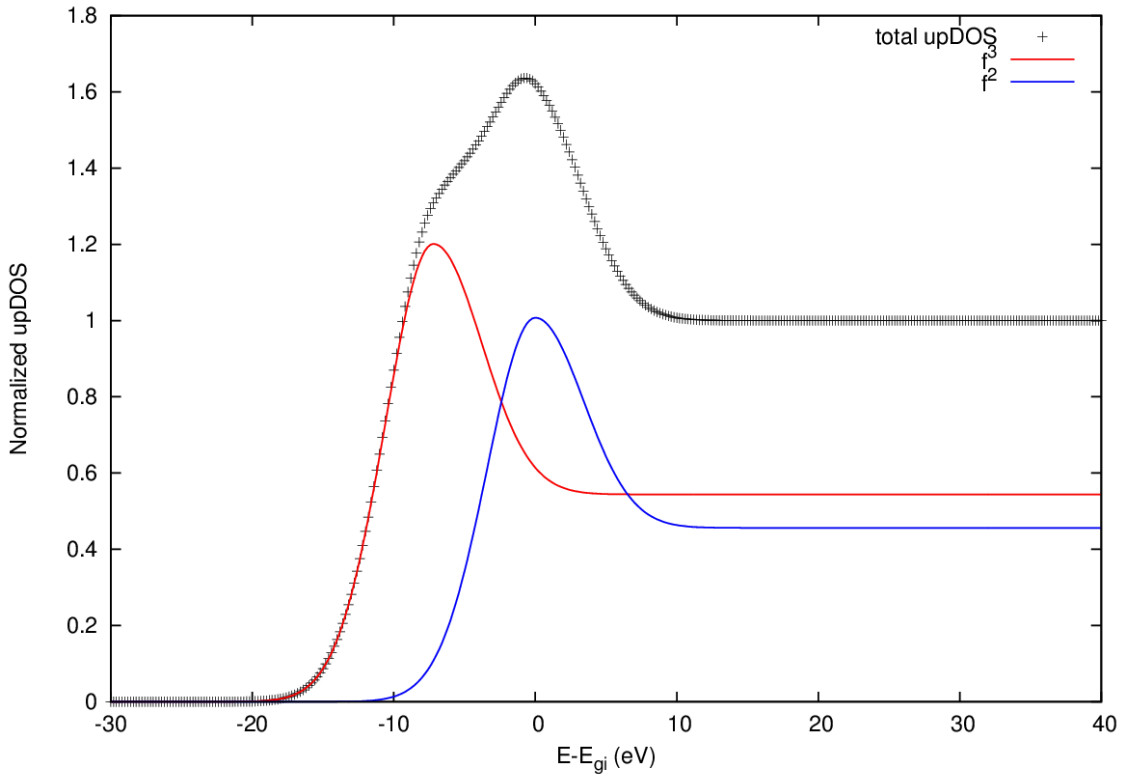
total upDOS
T3
T2
Normalized upDOS
E-Egi (eV)
1.8
1.6
1.4
1.2
1
0.8
0.6
0.4
0.2
0
-30
-20
-10
0
10
20
30
40

Fig. 4